Journal of Structural Geology, Vol. 9, No. 8, pp. 995 to 1005, 1987
Printed in Great Britain

0191-8141/87 $03.00 + 0.00

Atypical textures in quartz veins from the Simplon Fault Zone

NEIL S. MANCKTELOW

Geologisches Institut, ETH-Zentrum, CH-8092 Zürich, Switzerland

(*Received* 10 *November* 1986; *accepted in revised form* 1 *June* 1987)

Abstract—Samples of monomineralic quartz veins from the Simplon Fault Zone in southwest Switzerland and north Italy generally have asymmetric, single girdle *c*-axis patterns similar to textures measured from many other regions. Several samples have characteristically different textures, however, with a strong single *c*-axis maximum near the intermediate specimen axis *Y* (the direction within the foliation perpendicular to the lineation *X*) and a tendency for the other crystal directions to be weakly constrained in their orientation about this dominant *c*-axis maximum. This results in 'streaked' pole figure patterns, with an axis of rotation parallel to the *c*-axis maximum. These atypical samples also have a distinctive optical microstructure, with advanced recrystallization and grain growth resulting in a strong shape fabric (S_B) oblique to the dominant regional foliation (S_A), whereas typical samples have a strong S_A fabric outlined by very elongate, only partially recrystallized, ribbon grains. The recrystallized grains of the atypical samples are themselves deformed and show strong undulose extinction and a core–mantle recrystallization structure. The streaked texture is likely to be a direct consequence of lattice bending and kinking during heterogeneous slip on the favoured first-order prism $\{10\bar{1}0\}\langle a\rangle$ system, the heterogeneity itself being due to problems in maintaining coherence across grain boundaries when insufficient independent easy-slip systems are available for homogeneous strain by dislocation glide. Such bending would be particularly prevalent in very elongate, thin ribbon grains, resulting in high internal strain energy and promoting recrystallization. Thus both the texture and the microstructure could be significantly modified by later strain increments affecting quartz grains with an already developed, nearly single-crystal texture.

INTRODUCTION

THE STUDY of the crystallographic preferred orientation fabric (*texture*, cf. Weiss & Wenk 1985) of deformed rocks and minerals has proceeded over many years, with the implicit aim of providing constraints on the possible deformation path and kinematics (e.g. Sander 1948, 1970, Christie 1963, Law *et al.* 1984, 1986, Law 1986, Schmid & Casey 1986) and on the mechanisms of deformation (e.g. Tullis *et al.* 1973, Lister & Paterson 1979, Mancktelow 1987). The introduction of automated X-ray texture goniometers (e.g. Bunge & Wenk 1977, Schmid *et al.* 1981) and neutron diffraction analysis (e.g. Bouchez *et al.* 1979) has provided a further impetus by allowing more complete texture measurements and eliminating the otherwise total reliance on optically measurable directions. Quartz is a very common mineral in upper crustal rocks, often occurring in nearly monomineralic quartzites and quartz veins; it is not surprising that quartz textures have been frequently measured. From this large body of work has emerged a fairly standard range of observed textures for strongly deformed, quartz-rich rocks.

Samples from quartz veins collected within the Simplon Fault Zone in southwest Switzerland and north Italy generally display textures which are directly comparable with many already published patterns (Mancktelow 1985, 1987). Several samples from two widely separated locations (Fig. 1), however, show quite characteristic textures, which are different not only from those of the surrounding region but also from the range of previously published textures. These atypical patterns are streaked-out in a plane or cone of rotation about a single dominant *c*-axis orientation, rather than the discrete maxima observed in the more common textures. The atypical patterns are associated with a distinctive optical microstructure and are obviously the result of a change in one or more of the factors which control the developing texture (cf. Lister & Hobbs 1980, Schmid & Casey 1986, Mancktelow 1987). The study of the differences between these unusual textures and the more typical ones may therefore provide some insight into how such texture-controlling factors vary within a single major fault zone.

FIELD OCCURRENCE AND MEASUREMENT TECHNIQUES

The regional geology of the Simplon Fault Zone in the section between Simplonpass and Domodossola has been described in detail by Mancktelow (1985). The samples were collected from the well foliated, largely ductile deformed zone within the footwall block, which is separated from the hangingwall by a structural discontinuity (the 'Simplon Line'). Deformation within this section of the Simplon Fault Zone occurred under conditions of greenschist-facies metamorphism, with the growth of new chlorite and occasional biotite at the expense of earlier amphibolite-facies mineral assemblages. Samples SP107 and SP108 were collected within 10 m of each other, *ca* 3 km NW of the village of Simplon (Fig. 1). In this area there exists a late, variably developed kinking of the mylonite foliation about an axis at an acute angle (*ca* 25°) to the mylonitic elongation

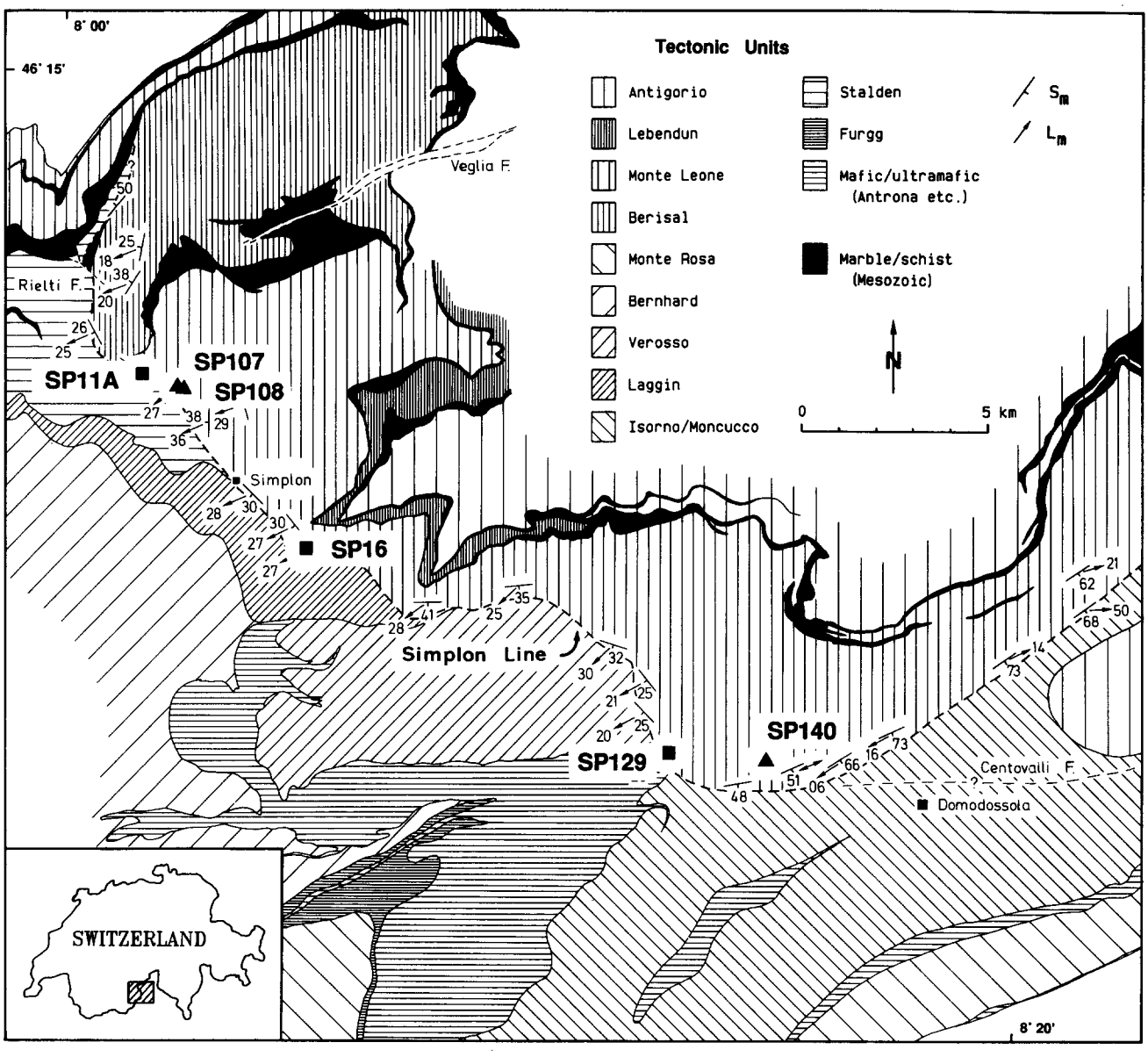

Fig. 1. Location map of the samples described. Square symbols indicate the typical samples, triangles the atypical samples. The simplified regional map of tectonic units is reproduced with permission from Mancktelow (1985).

lineation. Both specimens were selected from quartz veins in which this later effect was weak and the mylonitic foliation effectively planar. Such late folding is also developed in other areas along the Simplon Fault Zone which do not show the atypical quartz textures. SP140 was collected 20 km to the southeast (Fig. 1). These samples are unusually 'flinty', with a poorly developed foliation or banding compared to the more typical, strongly foliated mylonitic quartz veins. SP11A, SP16 and SP129 are discussed in Mancktelow (1987, Spec. Nos 4, 7 and 12) and represent examples of the more typical quartz textures. There is no immediately obvious relationship between the location of samples with atypical quartz textures and the geometry of the Simplon Fault Zone or its associated structures (Fig. 1).

The texture goniometer measurement techniques follow those of Schmid *et al.* (1981) and are summarized in Mancktelow (1987). The ODF calculations and associated regeneration of pole and inverse pole figures use the computer program package of Casey (1981).

Fig. 2. (a) Optical microstructure of sample SP16, which has a quartz texture typical of the Simplon Fault Zone. S_A is the dominant foliation as seen in the mylonitic gneisses containing the quartz veins, and defined in the veins themselves by elongate ribbon grains. S_B is the more weakly developed, oblique shape fabric defined by elongate recrystallized grains, subgrains and grain-boundary bulges (cf. Law *et al.* 1984, fig. 16). (b) Optical microstructure of one of the atypical samples, SP140. Note the much stronger development of the S_B foliation compared to (a). (c) An example of the recrystallization microstructure of the typical Simplon Fault Zone samples with elongate recrystallized new grains evenly distributed rather than concentrated at old grain boundaries. Specimen SP16, crossed polars. (d) Core–mantle microstructure consisting of cores of deformed larger, older grains (with undulose extinction and deformation bands) surrounded by a mantle of much finer grained, rather equant, recrystallized new grains. The microstructure is characteristic of the samples with atypical 'streaked' quartz textures. Specimen SP107, crossed polars.

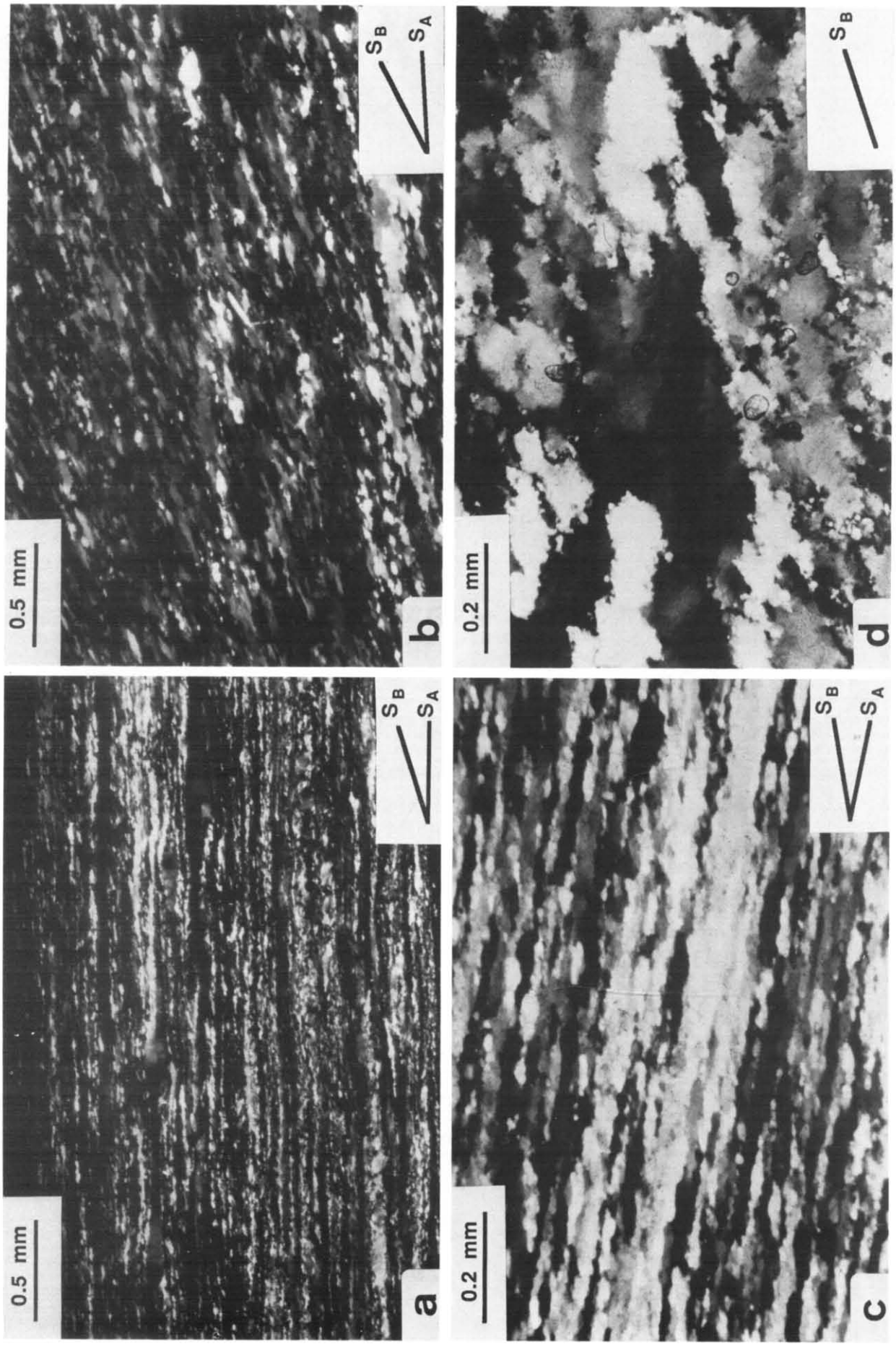

Fig. 2.

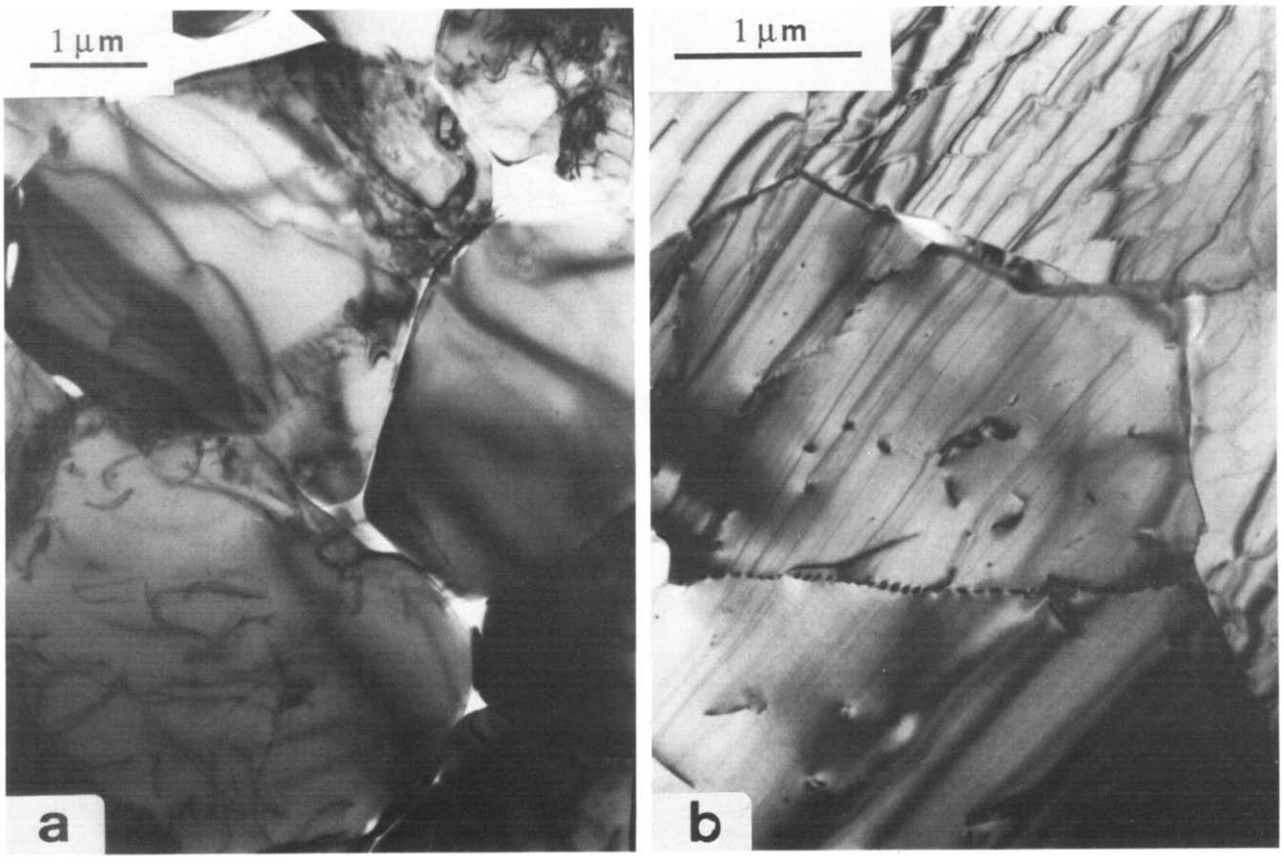

Fig. 3. Transmission electron photomicrographs showing the development of subgrains bounded by walls of dislocation arrays in samples with typical (SP11A, Fig. 3a) and atypical (SP140, Fig. 3b) quartz textures.

Optical *c*-axis measurements follow the methods of Turner & Weiss (1963). All data were contoured using programs modified after Starkey (1970).

The orthogonal *XYZ* specimen co-ordinate system used has the *Z* axis perpendicular to the foliation and the *Y* axis within the foliation and perpendicular to the mineral elongation lineation *X*. The photomicrographs and pole figures are all similarly oriented, with the foliation EW and vertical, the lineation horizontal, and the sense of shear dextral. All orientation data are displayed on equal area, upper hemisphere spherical projections in which the plane of projection contains the *X* (horizontal) and *Z* axes.

Transmission electron microscopy (TEM) was carried out with a Philips EM-400 125 kV microscope. Samples were taken from the rock slices previously used for transmission runs on the X-ray texture goniometer, and prepared by ion-thinning (cf. Barber 1970). As with previous studies, a major limitation was the rapidity of beam damage of quartz at higher magnifications.

OBSERVATIONS

Optical microstructure

Typical specimens from deformed quartz veins along the length of the Simplon Fault Zone (e.g. Fig. 2a & c) (Mancktelow 1987, fig. 2) generally show elongate to ribbon shaped 'old grains', with a dispersed development of elongate subgrains and new grains of grain size *ca* 80 μm, fairly regular boundaries, and weakly developed but distinct undulose extinction of the 'old grains'. The ribbon grains define a dominant grain-shape fabric S_A (cf. Law *et al.* 1984, figs. 16 and 17), which is parallel to the foliation measurable in the field. An additional shape fabric due to elongate subgrains, new grains and asymmetric grain-boundary bulges defines a much more weakly developed oblique foliation S_B (Fig. 2a & c) (Law *et al.* 1984). Shear bands are absent from quartz veins thicker than around 1 cm. Shear bands are strongly developed in the more micaceous matrix adjoining the quartz veins, but disappear within the first millimetre or so of the contact.

In contrast, the most immediate characteristic of the atypical samples is the weaker development of ribbon grains defining the main S_A foliation relative to the typical samples, and a correspondingly strongly developed S_B foliation (Fig. 2b) at an oblique angle of *ca* 15–20°. Ghosts of pre-existing ribbon grains defining S_A are seen as elongate bands of grains with a similar crystallographic orientation. The individual grains themselves are rather squat and are elongate in a direction defining S_B. The more equant shape of these grains gives the strong impression of a coarser average grain size than in the typical samples. The volume of individual, elongate ribbon grains in the typical samples, however, is at least as great as that for the more equant grains of the atypical samples. The apparent difference in grain size between typical and atypical samples is simply a shape effect.

The replacement of ribbon grains by more equant, relatively large grains, which are themselves elongate in a sense consistent with the imposed shear, indicates extensive dynamic recrystallization and grain growth in these samples (cf. Simpson & Schmid 1983). These large recrystallized grains themselves show a core–mantle recrystallization microstructure, with a mantle of fine (*ca* 10–30 μm), equant subgrains and new grains (Fig. 2d). Grain boundaries are very irregular, with an 'amoeboid' form suggesting active grain-boundary migration. The large grains show marked crystal lattice deformation with undulose extinction, deformation bands, kink bands and deformation lamellae. Occasional, narrow 'shear band' discontinuities filled with finer grained mica and quartz traverse the foliation at an angle of between 13 and 20°.

Textures

The measured and regenerated pole figures, optic *c*-axis figures and inverse pole figures for both typical and atypical 'streaked' textures are presented in Fig. 4. The *c*-axis textures of typical samples (Fig. 4a, p. 1000, Mancktelow 1987, fig. 2) show oblique, variably kinked single girdle patterns, often with vestiges of the crossed girdle form. Atypical textures (Fig. 4b, p. 1001) all show a strong preferred orientation of *c*-axes near, but not strictly parallel to the *Y* axis. As is best seen in the optical data, there is a tendency for the pattern to be elongated to form a limited segment of an oblique single girdle.

In the atypical specimens, the differences between the measured optical *c*-axis texture and the texture regenerated from the ODF give a clear example of the differing statistics of the two methods. The intensities calculated from the X-ray measurements are proportional to the volume of grains with a particular orientation in a thin slice parallel to the measured *XZ* face; the results show a strong single maximum with only a limited tendency to spread out along a girdle. In contrast, the optical *c*-axis textures are measurements of individual grains along spaced traverses in a single thin section, and are a function of the *number of grains* with a particular orientation rather than the *volume of material* with this orientation. This difference results in a bias towards a spread in *c*-axis orientations in the optical measurements compared to the X-ray measurements. Adjoining material with similar *c*-axis orientations are considered to be a

Fig. 4. Optic *c*-axes measured manually with a universal stage and *a* (poles to the second order prism $\{11\bar{2}0\}$), *m* (poles to the first order prism $\{10\bar{1}0\}$), and $r + z$ (poles to the positive $\{10\bar{1}1\}$ and negative $\{01\bar{1}1\}$ rhombs) measured by an automated X-ray texture goniometer, together with the mathematically regenerated *c*-axis pole figure (Casey 1981). Typical samples (SP11A, SP16 and SP129) in Fig. 4(a) (p. 1000), atypical samples (SP107, SP108 and SP140) in Fig. 4(b) (p. 1001).

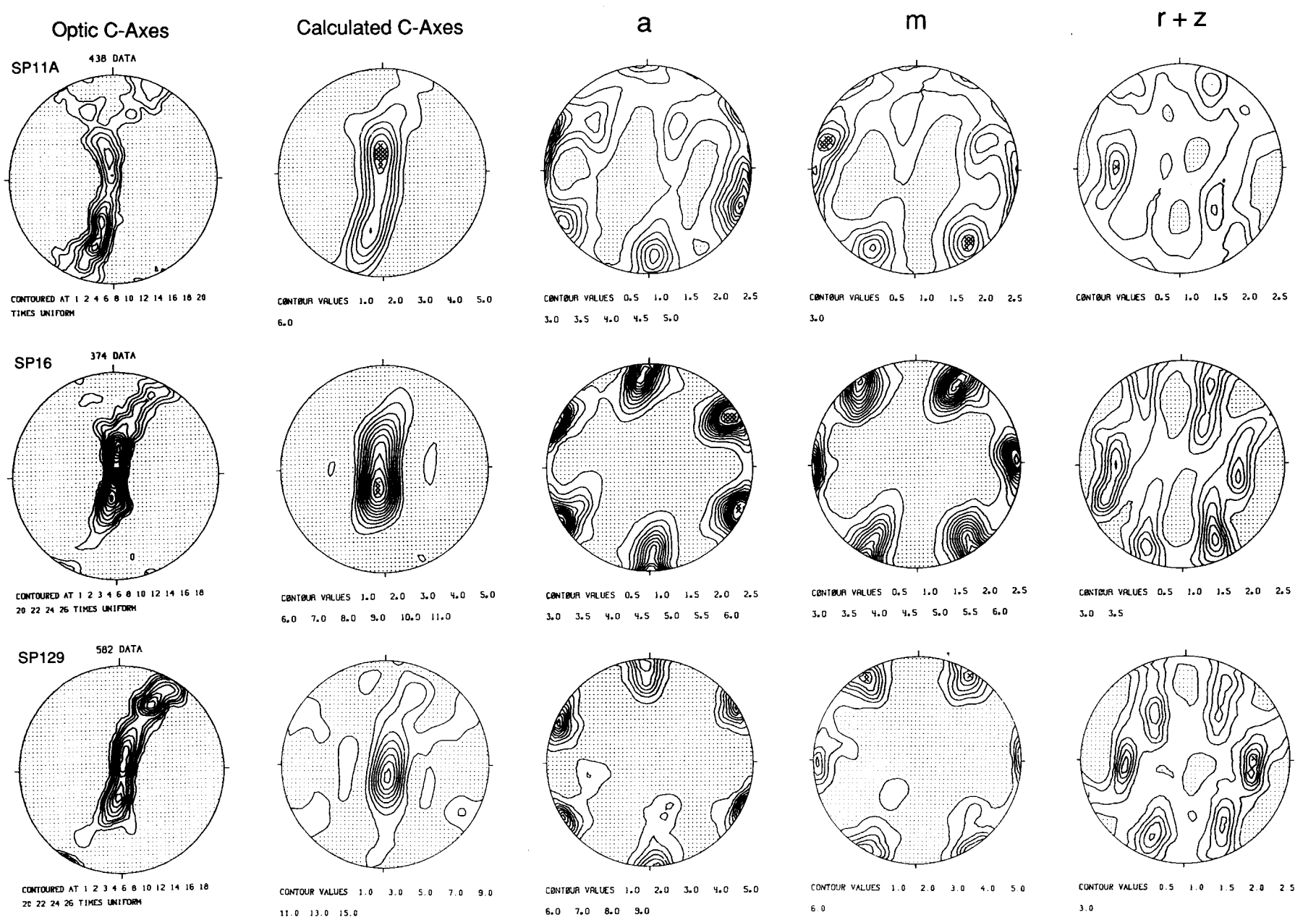
Optic C-Axes
Calculated C-Axes
a
m
r + z
SP11A
438 DATA
CONTOURED AT 1 2 4 6 8 10 12 14 16 18 20
TIMES UNIFORM
CONTOUR VALUES 1.0 2.0 3.0 4.0 5.0
6.0
CONTOUR VALUES 0.5 1.0 1.5 2.0 2.5
3.0 3.5 4.0 4.5 5.0
CONTOUR VALUES 0.5 1.0 1.5 2.0 2.5
3.0
CONTOUR VALUES 0.5 1.0 1.5 2.0 2.5
SP16
374 DATA
CONTOURED AT 1 2 3 4 6 8 10 12 14 16 18
20 22 24 26 TIMES UNIFORM
CONTOUR VALUES 1.0 2.0 3.0 4.0 5.0
6.0 7.0 8.0 9.0 10.0 11.0
CONTOUR VALUES 0.5 1.0 1.5 2.0 2.5
3.0 3.5 4.0 4.5 5.0 5.5 6.0
CONTOUR VALUES 0.5 1.0 1.5 2.0 2.5
3.0 3.5 4.0 4.5 5.0 5.5 6.0
CONTOUR VALUES 0.5 1.0 1.5 2.0 2.5
3.0 3.5
SP129
582 DATA
CONTOURED AT 1 2 3 4 6 8 10 12 14 16 18
20 22 24 26 TIMES UNIFORM
CONTOUR VALUES 1.0 3.0 5.0 7.0 9.0
11.0 13.0 15.0
CONTOUR VALUES 1.0 2.0 3.0 4.0 5.0
6.0 7.0 8.0 9.0
CONTOUR VALUES 1.0 2.0 3.0 4.0 5.0
6.0
CONTOUR VALUES 0.5 1.0 1.5 2.0 2.5
3.0

(a)

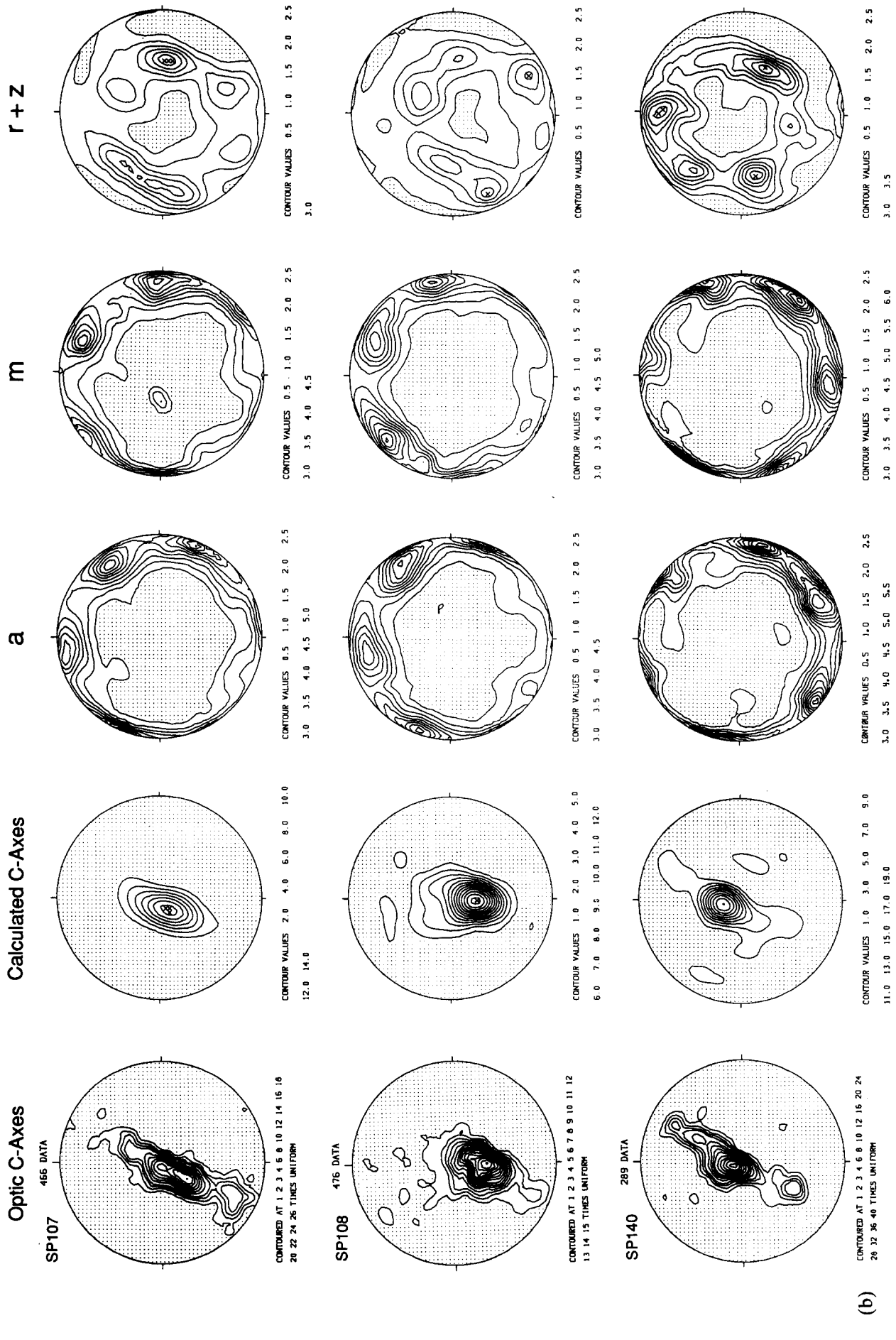
Optic C-Axes
Calculated C-Axes
a
m
r + z
SP107
465 DATA
CONTOURED AT 1 2 3 4 6 8 10 12 14 16 18 20 22 24 26 TIMES UNIFORM
CONTOUR VALUES 2.0 4.0 6.0 8.0 10.0 12.0 14.0
CONTOUR VALUES 0.5 1.0 1.5 2.0 2.5 3.0 3.5 4.0 4.5 5.0
CONTOUR VALUES 0.5 1.0 1.5 2.0 2.5 3.0 3.5 4.0 4.5
CONTOUR VALUES 0.5 1.0 1.5 2.0 2.5 3.0
SP108
476 DATA
CONTOURED AT 1 2 3 4 5 6 7 8 9 10 11 12 13 14 15 TIMES UNIFORM
CONTOUR VALUES 1.0 2.0 3.0 4.0 5.0 6.0 7.0 8.0 9.0 10.0 11.0 12.0
CONTOUR VALUES 0.5 1.0 1.5 2.0 2.5 3.0 3.5 4.0 4.5
CONTOUR VALUES 0.5 1.0 1.5 2.0 2.5 3.0 3.5 4.0 4.5 5.0
CONTOUR VALUES 0.5 1.0 1.5 2.0 2.5
SP140
289 DATA
CONTOURED AT 1 2 3 4 6 8 10 12 16 20 24 28 32 36 40 TIMES UNIFORM
CONTOUR VALUES 1.0 3.0 5.0 7.0 9.0 11.0 13.0 15.0 17.0 19.0
CONTOUR VALUES 0.5 1.0 1.5 2.0 2.5 3.0 3.5 4.0 4.5 5.0 5.5
CONTOUR VALUES 0.5 1.0 1.5 2.0 2.5 3.0 3.5 4.0 4.5 5.0 5.5 6.0
CONTOUR VALUES 0.5 1.0 1.5 2.0 2.5 3.0 3.5
(b)

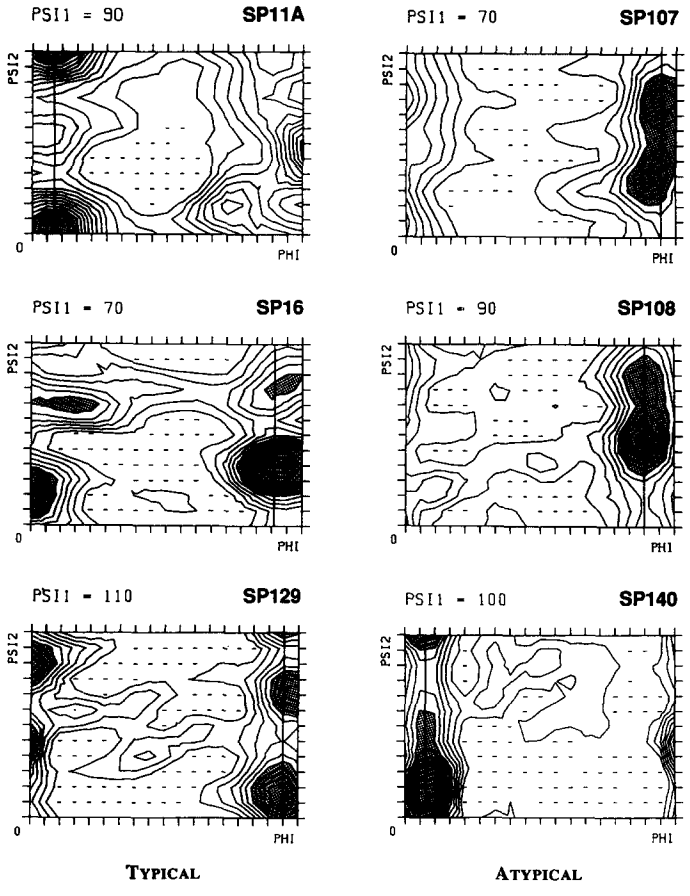

Fig. 5. Two-dimensional sections through the three-dimensional orientation distribution function (ODF) (cf. Casey 1981). The Euler angles PSI1 and PHI fix the *c*-axis orientation and the marked straight line traverses of constant PSI1 and PHI therefore represent single *c*-axis orientations which correspond to the maximum intensities of the calculated *c*-axis pole figures of Fig. 4.

single 'grain', although there may be considerable, optically indetectable, discrepancy in the orientation of crystal axes other than *c*. The differing measurement statistics of the two methods provide complementary rather than purely correlatory results. By comparison of the two methods, it is clear that the natural textures for the unusual samples have an overwhelming volume of material with a similar *c*-axis orientation close to the *Y*-axis and an important, albeit volumetrically less significant, minority of grains that define a fairly straight single girdle inclined at 25–30° to the foliation and lineation.

The *c*-axis pole figures from these atypical samples, while consistently distinctive, differ only in degree from many others measured along the Simplon Fault Zone (cf. specimen SP16, Fig. 4a). The characteristic which sets these samples apart is most clear in the pole figures for lattice directions other than *c* and from the ODF sections. The typical textures for *a*, *m* and *r* + *z* (Fig. 4a, Mancktelow 1987) have distinct intensity maxima, similar in form and orientation to textures reported from other regions by Bouchez (1978, fig. 1), Behrmann & Platt (1982, fig. 6), Law *et al.* (1986) and Schmid & Casey (1986, figs. 5 and 15). Ridges of moderate intensity joining these maxima, when present, are related to a single dominant *a* maximum within the *XZ* plane, at an angle of *ca* 25° to the lineation (e.g. Mancktelow 1987, fig. 6). The *a*, *m* and *r* + z textures for the atypical samples (Fig. 4b) also show intensity maxima which are similar in orientation to the typical samples. However, they display clear intensity ridges, representing a smaller but still clearly significant volume of grains, concentric about the dominant *c*-axis orientation near the *Y* specimen axis. This is seen as a 'streaking' of the *a* and *m* intensity contours in a plane perpendicular to the dominant *c*-axis orientation, and of the *r* + *z* intensity contours in a cone about this axis (Fig. 4b). In the ODF representation (Fig. 5), the position of the *c*-axis is fixed by the Euler angles PSI1 and PHI, while the angle PSI2 defines the orientation of the other lattice directions about this fixed *c*-axis orientation (cf. Casey 1981, Schmid *et al.* 1981). The streaking of the pole figures is, therefore, clear in the ODF sections as a tendency for the PSI2 angle to be less well defined (for constant PSI1 and PHI) in the atypical samples than in the more common examples (Fig. 5).

Transmission electron microscopy

Under the TEM, samples with both typical and atypical quartz textures are very heterogeneous. They show a complete range of microstructures: 'old grains' with high free dislocation densities, grains with a well developed polygonal substructure, subgrains bounded by walls of

ordered dislocations and small (4–8 μm) 'new grains' with narrow, straight, high-angle grain boundaries (Fig. 3). In all samples, the dominant mechanism of recrystallization appears to be subgrain rotation.

All samples have a high pore concentration along grain boundaries and especially at grain boundary triple points (e.g. Fig. 3a). Pores within grains are relatively rare and are generally associated with dislocation nodes or arrays, apparently pinning the dislocations. By analogy with little deformed quartz veins away from the Simplon Fault Zone, the initial intragranular fluid inclusion content of the vein quartz was high. In the present, highly deformed samples this fluid is concentrated on the grain boundaries, probably due to a collection of these fluid inclusions on mobile grain boundaries sweeping through the material. The fluids must then diffuse as impurities with the grain boundary and this diffusion will be the rate-controlling step for grain-boundary migration (cf. Poirier 1985).

DISCUSSION

Consider first the possibility that the streaking is related to the bulk deformation geometry and therefore to the specimen co-ordinate axes XYZ. Streaking about the Y axis implies that the X and Z directions lose their significance. In the extreme case of a texture completely streaked about Y, as far as the texture pattern is concerned, the only significant axis is Y. Such a textural transition is unlikely to be due to the finite-strain geometry, where the possible range is from true flattening (Flinn parameter $k = 0$), with a single significant shortening axis, to true constriction ($k = \infty$), with only the extension axis significant. The intermediate axis can never be the only significant finite strain axis.

Another possible explanation of the observed textures could be provided by the addition of grain-boundary sliding to the active deformation mechanisms in these samples, as shown in Fig. 6. Grains with their c-axes parallel to the intermediate specimen axis Y will have had a high resolved shear stress on the prism $\{10\bar{1}0\}\langle a\rangle$ slip system, which is a system of easy slip at moderate temperatures (e.g. Linker *et al.* 1984). If deformation was heterogeneous on the grain-scale, such grains could deform by a combination of intracrystalline dislocation glide on this system and diffusion-controlled grain-boundary sliding. Strain hardening within individual grains during dislocation glide could produce grains which are 'harder' than their neighbours. These may then rotate as semi-rigid particles, accommodated by grain-boundary sliding, until a new 'softer' orientation of the intracrystalline slip system is attained (Fig. 6), at which time they would become soft matrix grains to other hard, rotating grains, and so on in a continuous cycle. This mechanism would maintain a stable c-axis orientation parallel to the axis of rotation (the Y axis), but involve a rotation of the other crystallographic directions about this axis.

The major argument against such a mechanism is

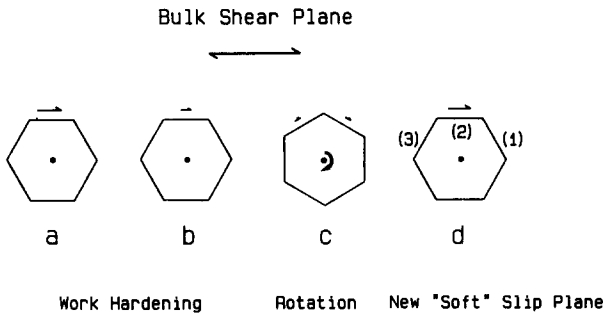

Fig. 6. Hypothetical mechanism for combined prism $\{10\bar{1}0\}\langle a\rangle$ slip and rotation associated with grain-boundary sliding. A single quartz crystal has three such slip planes available with 60° between them.

provided by the optic c-axis textures. It is clear from Fig. 4(b) that the c-axes away from the central Y specimen axis define a clear single girdle and are not themselves rotated about Y. Rather, it appears that the 'streaking' occurs around the dominant c-axis orientation maximum and not about a particular specimen axis. It follows that the mechanism of 'streaking' must be controlled by the crystallography of individual grains and not *directly* by the kinematics or geometry of the imposed deformation.

The most likely explanation may be found in the observation that the atypical textures show extensive internal strain features within the volumetrically dominant larger grains (undulose extinction, deformation bands, etc.). As noted above, grains with c-axis orientations near the Y specimen axis are favoured for slip on the prism $\{10\bar{1}0\}\langle a\rangle$ system. Kinking and bending of grains utilizing this slip system will involve an axis of external rotation within the slip plane and perpendicular to the a slip direction: that is, the c-axis (cf. Vernon 1976, fig. 6.2). Tilt walls consisting of an array of edge dislocations will have the same axis of external rotation (Vernon 1976, fig. 6.7a, Poirier 1985, fig. 2.17), as will new grains developed by continued subgrain rotation across such walls. None of these rotations will be optically visible, as they do not affect the orientation of the optic c-axis. However, in the complete X-ray textures this will be seen as a rotation of the other crystallographic directions around a common c-axis—which is exactly what is observed in the atypical examples. White (1976) studied the angular relationships between old and new recrystallized grains using selected area diffraction patterns under the TEM. His results indicate a rotation around a common a axis rather than c, as postulated for the atypical Simplon Fault Zone samples. This may suggest that basal slip was more important in his sample, but the texture of the studied sample was not published and direct comparison is not possible.

Why is this intracrystalline bending only observed in a few 'atypical' examples? If the streaking effect is ignored, the texture of the atypical samples quite closely approximates a single crystal orientation, with the c-axis oriented nearly parallel to the intermediate specimen axis Y. As noted above, in this orientation there is a high resolved shear stress on the $\{10\bar{1}0\}\langle a\rangle$ slip system. However, $\{10\bar{1}0\}\langle a\rangle$ provides only two independent slip

systems—too few for a general homogeneous deformation (which would require five, cf. Paterson 1969). Because a large volume per cent of the quartz grains have an almost identical crystallographic orientation, there is little freedom for varying and distributing the deformation between different grains in order to circumvent this restriction. The grains themselves, therefore, tend to kink and bend internally, providing the heterogeneous deformation required to maintain coherence while undergoing a progressive bulk strain. As discussed above, this heterogeneous crystal bending will be seen as a 'streaking' of the quartz textures about the predominant *c*-axis orientation. Such high internal strains would promote dynamic recrystallization, leading to the observed strongly recrystallized optical microstructure. Very elongate, thin ribbon grains would be particularly susceptible to intracrystalline bending and would be preferentially eliminated from the microstructure by recrystallization in favour of more equant grains. The crystal bending is necessary to maintain coherence across grain boundaries in a material with insufficient easy slip systems to accommodate the imposed deformation by dislocation glide alone. It follows that a larger equilibrium grain size, with a lower grain-boundary area to volume ratio, is advantageous, favouring dynamic grain growth in association with recrystallization.

Typical samples (e.g. Fig. 4a), in which there is a range of grain orientations, provide the rock with more variably oriented easy slip systems, allowing more freedom to distribute the strain heterogeneously between grains rather than bending individual grains. The problem of maintaining coherence across grain boundaries is therefore less acute and a microstructure develops which is most advantageous for continued dislocation glide. Grain boundaries, acting as a sink for dislocations, are now an aid to easy deformation and grain growth is inhibited, resulting in a smaller average recrystallized grain size. Very elongate ribbon grains, oriented for easy slip and thereby providing a geometric softening mechanism, are retained.

The optical microstructure, the strong single *c*-axis maximum texture and the 'streaking' of the other crystal directions around *c* are therefore logically interrelated. Significantly, specimen GRAN 133 of Schmid & Casey (1986), which differs from all their other measured samples in having a very strong single *c*-axis maximum near the *Y* specimen axis, also shows very similar *a*, *m*, *r* and *z* patterns to the atypical textures from the Simplon Fault Zone, though the streaking about the *c*-axis maximum is less pronounced. The texture in this granulite specimen is considered to have formed under retrograde amphibolite-facies conditions (Behr 1961, 1965), in contrast to texture formation under retrograde greenschist-facies conditions along the Simplon Fault Zone. These rather unusual textures may therefore develop over a broad range of metamorphic conditions.

The atypical microstructure, with advanced recrystallization and extensive undulose extinction, and the streaking of the textures is considered to post-date, and be dependent upon, the development of a practically single-crystal quartz texture. This modification of the microstructure and texture may well be part of a continuing or even repetitive process. That the overprint occurred with the same kinematics as the general Simplon movements (cf. Mancktelow 1985) is obvious from the consistent asymmetry to the quartz grain shape fabrics and textures in both typical and atypical examples. The optical evidence for advanced recrystallization and grain growth in the atypical samples suggests that at least part of the overprint occurred within the hot-working regime, as does the clear evidence for recovery (dislocation walls, subgrains and new grains) under the TEM. The initial nearly single crystal orientation would be very favourable for plane strain simple shear, as only two independent slip systems are required for homogeneous plane strain if the slip directions lie within the *XZ* plane. Deformation could then occur by simplex or duplex slip on the $\{10\bar{1}0\}\langle a\rangle$ system (Mancktelow 1987, Schmid *et al.* 1981). However, if the later increment was not plane strain or if the shear direction changed slightly, then the strain increment could not be readily accommodated by the strongly textured material. Average stress levels would be higher, and the bending and kinking discussed above could develop, leading in turn to a modification of the optical microstructure and the observed streaking of the texture.

CONCLUSION

The textures considered here are presented as unusual examples, which are clearly different from the general patterns established both by previous workers and by study along the Simplon Fault Zone. These atypical textures are associated with an equally distinctive optical microstructure, with advanced recrystallization and grain growth at the expense of ribbon grains (though grain growth/grain size may be somewhat overestimated optically due to many grains having common *c*-axis orientations), well developed core–mantle structure and extensive undulose extinction. The observed crystallographic preferred orientation and microstructure are mutually consistent. For grains with *c*-axes near parallel to the intermediate axis *Y*, the most likely easy slip system is the prism $\{10\bar{1}0\}\langle a\rangle$. With such a slip system operating, kinking and bending of the crystal lattice will generally occur with an axis of external rotation parallel to *c*. If subgrains and new grains develop by continued rotation of the bent crystal lattice, the axis of rotation between host and subgrains or new grains will also be approximately *c*. It follows that the observed 'streaking' or rotation of the other crystal axes about the *c*-axis in the measured textures may be directly related to the observed microstructural development of strongly bent grains and advanced recrystallization. It is significant that many of the crystal lattice rotations will be indiscernible optically, as they have the *c*-axis (the only optic axis in quartz) as their axis of rotation. The extent of these rotations is only clear from the X-ray texture measurements of crystal axes other than *c*, providing another

clear example of the usefulness of full texture determinations (cf. Schmid *et al.* 1981).

Acknowledgements—Particular thanks are due to David Olgaard, who carried out the preliminary TEM study on samples from the Simplon Fault Zone. David Mainprice, Rick Law, David Olgaard and Stefan Schmid are thanked for their thorough and constructive reviews of various drafts of the manuscript and Martin Casey and Rick Law for general discussions which helped clarify the ideas presented here. Financial support from the Schweizerischer Nationalfonds, Project No. 2.556-0.84 is gratefully acknowledged.

REFERENCES

Barber, D. J. 1970. Thin foils of non-metals made for electron microscopy by sputter-etching. *J. Mater. Sci.* **5**, 1–8.

Behr, H. J. 1961. Beiträge zur petrographischen und tektonischen Analyse des sächsischen Granulitgebirges. *Freiberger Forschft.* **C119**, 1–146.

Behr, H. J. 1965. Zur Methodik tektonischer Forschung im kristallinen Grundgebirge. *Ber. geol. Ges. DDR* **10**, 163–179.

Behrmann, J. H. & Platt, J. P. 1982. Sense of nappe emplacement from quartz *c*-axis fabrics; an example from the Betic Cordilleras (Spain). *Earth Planet. Sci. Lett.* **59**, 208–215.

Bouchez, J. L. 1978. Preferred orientations of quartz *a* axes in some tectonites: kinematic inferences. *Tectonophysics* **49**, T25–T30.

Bouchez, J. L., Dervin, P., Mardon, J. P. & Englander, M. 1979. La diffraction neutronique appliquée à l'étude de l'orientation préférentielle de réseau dans les quartzites. *Bull. Minéral.* **102**, 225–231.

Bunge, H. J. & Wenk, H. R. 1977. Three-dimensional texture analysis of three quartzites (trigonal crystal and triclinic specimen symmetry). *Tectonophysics* **40**, 257–285.

Casey, M. 1981. Numerical analysis of X-ray texture data: an implementation in FORTRAN allowing triclinic or axial specimen symmetry and most crystal symmetries. *Tectonophysics* **78**, 51–64.

Christie, J. M. 1963. The Moine thrust zone in the Assynt region, northwest Scotland. *Calif. Univ. Publ. geol. Sci.* **40**, 345–440.

Law, R. D. 1986. Relationships between strain and quartz crystallographic fabrics in the Roche Maurice quartzites of Plougastel, western Brittany. *J. Struct. Geol.* **8**, 493–515.

Law, R. D., Casey, M. & Knipe, R. J. 1986. Kinematic and tectonic significance of microstructures and crystallographic fabrics within quartz mylonites from the Assynt and Erribol regions of the Moine thrust zone, NW Scotland. *Trans. R. Soc. Edinb., Earth Sci.* **77**, 99–125.

Law, R. D., Knipe, R. J. & Dayan, H. 1984. Strain path partitioning within thrust sheets: microstructural and petrofabric evidence from the Moine Thrust Zone at Loch Eriboll, northwest Scotland. *J. Struct. Geol.* **6**, 477–497.

Linker, M. F., Kirby, S. H., Ord, A. & Christie, J. M. 1984. Effects of compression direction on the plasticity and rheology of hydrolytically weakened synthetic quartz crystals at atmospheric pressure. *J. geophys. Res.* **89**, B6, 4241–4255.

Lister, G. S. & Hobbs, B. E. 1980. The simulation of fabric development during plastic deformation and its application to quartzite: the influence of deformation history. *J. Struct. Geol.* **2**, 355–370.

Lister, G. S. & Paterson, M. S. 1979. The simulation of fabric development during plastic deformation and its application to quartzite: fabric transitions. *J. Struct. Geol.* **1**, 99–115.

Mancktelow, N. S. 1985. The Simplon Line: a major displacement zone in the western Lepontine Alps. *Eclog. geol. Helv.* **78**, 73–96.

Mancktelow, N. S. 1987. Quartz textures from the Simplon Fault Zone, southwest Switzerland and north Italy. *Tectonophysics* **135**, 133–153.

Paterson, M. S. 1969. The ductility of rocks. In: *Physics of Strength and Plasticity* (edited by Argon, A. S.). M.I.T. Press, Cambridge, Massachusetts, 377–392.

Poirier, J. P. 1985. *Creep of Crystals*. Cambridge University Press, Cambridge.

Sander, B. 1948. *Einführung in die Gefügekunde der geologischen Körper*. Springer-Verlag, Wien.

Sander, B. 1970. *An Introduction to the Study of Fabrics of Geological Bodies*. Translated from the German by F. C. Phillips and G. Windsor. Pergamon Press, Oxford.

Schmid, S. M. & Casey, M. 1986. Complete fabric analysis of some commonly observed quartz *c*-axis patterns. In: *Mineral and Rock Deformation: Laboratory Studies, The Paterson Volume* (edited by Hobbs, B. E. & Heard, H. C.). *Am. geophys. Un. Monogr.* **36**, 263–286.

Schmid, S. M., Casey, M. & Starkey, J. 1981. An illustration of the advantages of a complete texture analysis described by the orientation distribution function (ODF) using quartz pole figure data. *Tectonophysics* **78**, 101–117.

Simpson, C. & Schmid, S. M. 1983. An evaluation of criteria to deduce the sense of movement in sheared rocks. *Bull. geol. Soc. Am.* **94**, 1281–1288.

Starkey, J. 1970. A computer programme to prepare orientation diagrams. In: *Experimental and Natural Rock Deformation* (edited by Paulitsch, P.). Springer, New York, 51–74.

Tullis, J. A., Christie, J. M. & Griggs, D. T. 1973. Microstructures and preferred orientations of experimentally deformed quartzites. *Bull. geol. Soc. Am.* **84**, 297–314.

Turner, F. J. & Weiss, L. E. 1963. *Structural Analysis of Metamorphic Tectonites*. McGraw-Hill, New York.

Vernon, R. H. 1976. *Metamorphic Processes. Reactions and Microstructure Development*. George Allen & Unwin, London.

Weiss, L. E. & Wenk, H.-R. 1985. An Introduction. In: *Preferred Orientation in Deformed Metals and Rocks: An Introduction to Modern Texture Analysis* (edited by Wenk, H.-R.). Academic Press, Orlando, 1–10.

White, S. H. 1976. The effects of strain on the microstructures, fabrics and deformation mechanisms in quartzites. *Phil. Trans. R. Soc. Lond.* **A283**, 69–86.

APPENDIX

Specimen locations

Grid co-ordinates refer to the Swiss national topographic map series, published by the Bundesamt für Landestopographie. The collection code refers to the numbering of specimens stored in the Geologisches Institut, ETH Zürich, Switzerland.

Grid co-ordinates	Collection code
64470.11935	SP11A
64921.11437	SP16
65900.10909	SP129
64564.11880	SP107
64564.11878	SP108
66208.10860	SP140